



Paper 26: 4.6

## COMPUTATION OF FLOW THROUGH VENTURI METERS

**Authors:**

Jane A. Sattery and Michael J. Reader-Harris, Flow Center NEL, U.K.

**Organiser:**

Norwegian Society of Chartered Engineers  
Norwegian Society for Oil and Gas Measurement

**Co-organiser:**

National Engineering Laboratory, UK

Reprints are prohibited unless permission from the authors  
and the organisers

# COMPUTATION OF FLOW THROUGH VENTURI METERS

by

Jane A. Sattary and Michael J. Reader-Harris

Flow Centre  
NEL  
East Kilbride  
Glasgow, G75 0QU, UK

## SUMMARY

The computational fluid dynamics (CFD) work on Venturi meters reported in this paper was part of a large project for Shell Exploration and Production to investigate the application of Venturi meters to gas flow measurement. The majority of the experimental findings were reported in 'Unpredicted behaviour of Venturi flowmeters in gas at high Reynolds numbers' presented in the 1996 North Sea Flow Metering Workshop.

CFD has been used to model the flow through Venturi tubes and thereby gain understanding of how the discharge coefficient is affected by the vital parameters of diameter ratio, pipe Reynolds number and roughness. It has also been used to calculate the effect of manufacturing tolerance. The discharge coefficients obtained from the calibration of Venturi meters have been used to validate the CFD predictions. The CFD results have also been compared with experimental results from the 1950s and 1960s with surprisingly good agreement.

This work forms the basis of further possible research using CFD on the effect of upstream and Venturi surface roughness on the performance of these meters. The knowledge gained on the effect of surface roughness may also be applicable to ultrasonic flowmeters.

## 1 INTRODUCTION

The oil and gas industry has in recent years shown a substantial interest in using Venturi meters as part of multiphase flow metering systems and particularly in wet gas metering applications. Much of this interest has stemmed from the basic understanding that Venturi flowmeters are rugged industrial devices which utilise a well established model of fluid flow to derive a fluid flowrate from a measurement of differential pressure. A high accuracy metering system for wet gas was described by Dickinson and Jamieson<sup>(1)</sup> in October 1993 and showed that use of this system rather than a conventional separation system could mean the difference between a marginal field being viable or not. The system utilized Venturis as the primary elements and used Murdock's<sup>(2)</sup> equation to correct for wet gas effects.

Shell Expro had an application for such a metering system which required an overall uncertainty close to that for gas fiscal metering systems. The installation would be operating at Reynolds numbers in the range  $10^6$  to  $10^7$ , well above the upper range limit ( $10^6$ ) stated in the Standard<sup>(3)</sup> for Venturi meters. Shell Expro accepted that the Venturi meters should be calibrated in liquid and gas to give baseline discharge coefficients. NEL was commissioned by Shell Expro to carry out the calibrations and also to carry out an independent parallel computer simulation study.

The Computational Fluid Dynamics (CFD) study was used to interpret and extend the experimental work: it examined the effect of changes in geometry, Reynolds number and roughness on the discharge coefficient of Venturi meters. The results of the simulations are presented in this paper. The CFD results are validated against the baseline calibrations carried out at NEL in water and also compare well with experimental and theoretical work on Venturi meters carried out in the 1950s and 1960s.

## 2 GEOMETRY AND SPECIFICATIONS

In the experimental programme the Venturi baseline calibrations in water were to be carried out first and so the computations were set up to simulate these calibrations as closely as possible so that direct baseline comparisons could be made.

**Baseline cases similar to those in the experimental tests in water were computed for smooth Venturi tubes with pipe diameter,  $D = 154.04$  mm and Reynolds number,  $Re_D = 10^6$  for three different diameter ratios:  $\beta = 0.4, 0.6$  and  $0.75$ .**

The Venturi tubes consisted of an entrance section of length  $2D$ , a convergent section of included angle  $21^\circ$ , a throat section of length  $1d$ , a divergent section of included angle  $7.5^\circ$  and an outlet section of length  $2D$ . The pressure tapping holes were not modelled.

The radius of curvature on the intersection of the divergent section and the downstream section was always zero: the radius of curvature on all other corners was 5 mm (this is the smallest radius that could reasonably be obtained at the time).

The density,  $\rho$ , was specified as  $10^3 \text{ kg/m}^3$  and the viscosity,  $\mu$ , was  $10^{-3} \text{ Pa s}$ . The mass flowrate,  $q_m$ , was  $120.4 \text{ kg/s}$  giving a mean pipe velocity,  $\bar{u}$ , of  $6.46 \text{ m/s}$ .

### 3 BASELINE RESULTS

#### 3.1 CFD Results

Figs 1 and 2 show the profiles along the length of the Venturi tube for  $\beta = 0.4$  (on the graphs zero on the x-axis is at the Venturi tube inlet 2D upstream of the convergent section). Fig. 1 shows the velocity profiles along the length of the Venturi tube. The smooth profile is along the centreline with the peak at the throat. The mean velocity through the throat section was  $40.37 \text{ m/s}$ . The spiky profile is close to the wall: the discontinuities occur at the points adjacent to the corners of the Venturi tube. The maximum velocity at the intersection of the convergent and the throat section was  $44.5 \text{ m/s}$ .

Fig. 2 shows the static pressure profiles along the length of the Venturi tube: again the smooth profile is along the centreline and the spiked profile is along the wall; note that the static pressure is almost constant across the Venturi tube at the throat tapping, whereas at the corners it changes very substantially with radial position. The static pressure drops from  $1.01019 \times 10^5 \text{ Pa}$  at the upstream wall tapping position to  $-7.18045 \times 10^5 \text{ Pa}$  at the throat tapping position giving a differential pressure of  $8.19064 \times 10^5 \text{ Pa}$ .

The static pressure profiles are shown in detail in Fig. 3. The static pressure is at a minimum at the intersection of the convergent and throat section and is  $-1.04 \times 10^6 \text{ Pa}$ , 41 per cent lower than that at the throat. However, the positioning of the throat tapping is not critical since even at a distance of  $1/4$ d upstream of the throat tapping position the static pressure has decreased by only 1.2 per cent. The spike at each intersection did not just occur close to the wall: it persisted into the flow as shown by the three smoother profiles in Fig. 3; only at approximately  $5 \text{ mm}$  ( $\approx 0.1$ d) from the wall did the static pressure adjacent to the corner equal that at the throat tapping.

#### 3.2 Comparison With Experimental Results

The discharge coefficients obtained computationally,  $C_{\text{CFD}}$ , for the three diameter ratios were compared with those obtained experimentally,  $C_{\text{EXP}}$ , in water and are given in Table 1. The three Venturi tubes used in the water calibrations were manufactured to meet the requirements of BS EN ISO 5167-1<sup>(3)</sup>; also it should be noted that for  $\beta = 0.4$  the maximum measured Reynolds number was less than  $10^6$ . Table 1 also gives the percentage difference in discharge coefficient between computation and experiment,  $\Delta C_{p,\text{EXP}}$ , and between  $C_{\text{CFD}}$  and  $C$  given in BS EN ISO 5167-1,  $\Delta C_{p,\text{ISO}}$ .

TABLE 1

PERCENTAGE DIFFERENCE IN DISCHARGE COEFFICIENT

$\beta$	$C_{CFD}$	$C_{EXP}$	$C_{ISO}$	$\Delta C_{p,EXP}$	$\Delta C_{p,ISO}$
0.4	0.98463	0.9912	0.995	-0.66	-1.04
0.6	0.98618	0.9895	0.995	-0.34	-0.89
0.75	0.98637	0.9981	0.995	-1.18	-0.87

For a Classical Venturi tube with a machined convergent section the Standard specifies a discharge coefficient of 0.995 for all the diameter ratios. The agreement between computational and experimental results is surprisingly good, considering the discharge coefficients obtained from the Venturis in the experimental results differed within themselves by 0.9 per cent.

A major reason for the measured results always being higher than those computed is that the measurements are affected by the fact that the pressure tapping holes are sufficiently large that the measured static pressures are larger than those which would be obtained with a pressure transducer flush mounted on the wall. The measured differential pressure is smaller and the measured discharge coefficient larger than would be obtained in an experiment totally similar to the computational model. Further work is being done to quantify this effect.

### 3.3 Comparison With Earlier Experimental Work

The severe discontinuities in the pressure profile at the inlet and exit of the throat in the CFD results were observed some thirty years earlier experimentally by Lindley<sup>(4)</sup>. Lindley measured the wall pressure distribution along a Venturi with air as the working fluid. The results, Fig. 4, clearly show a strong adverse pressure gradient at the throat inlet which indicates the possibility of separation. The throat inlet section is shown in more detail by Lindley and reproduced in Figs 5 and 6 for throat Reynolds numbers,  $Re_d$ , below  $3 \times 10^5$  and above  $3 \times 10^5$  respectively. With the lower values of  $Re_d$  there is a clear flat spot downstream of the throat inlet. Lindley believed this was a clear indication of a separation bubble and subsequently proved the existence of a bubble at low values of  $Re_d$  by performing experiments with a perspex Venturi meter. However, this phenomenon was not seen at the higher values of  $Re_d$  shown in Fig. 6 and so Lindley concludes that no separation is expected to occur in this case. Lindley found similar results with water as the working fluid; there was evidence of separation but only for  $Re_d$  lower than about  $2 \times 10^5$ .

Following Lindley's conclusions no separation was expected for the baseline computations where  $Re_d$  ranged from  $1.3 \times 10^6$  to  $2.5 \times 10^6$ . No flat spots were observed in the wall pressure profiles (Fig. 3) and there was no evidence of separation in any of the computations.

#### 4 EFFECT OF COMPRESSIBLE FLOW

All baseline computations were carried out with incompressible flow specified in order to compare with the Venturi calibrations in water. When the Venturi meters were calibrated in high pressure gas in the next part of the experimental programme unexpected discharge coefficients were obtained; many of the discharge coefficients were greater than unity. An extensive investigation to determine the cause of this behaviour was undertaken by NEL and reported by Jamieson<sup>(5)</sup> in the 1996 North Sea Flow Metering Workshop. Prior to these results it was believed that for the computations the discharge coefficients would be identical for incompressible and compressible flows when computed at the same Reynolds number. To confirm this belief additional computations were performed to determine the effect of compressible flow at a similar Reynolds number to that of the calibrations in gas.

The incompressible flow computations were carried out with a structured mesh, however this technique was unsuitable for the computation of compressible flow through Venturis, therefore an unstructured grid was required to obtain a solution for compressible flows. Using the unstructured mesh a comparison was made between compressible and incompressible flow for  $\beta = 0.4$ ,  $Re_D = 2.66 \times 10^6$ ,  $D = 154.04$  mm,  $q_m = 5.8$  kg/s and at the inlet  $\bar{u} = 12.68$  m/s,  $\rho = 24.4$  kg/m<sup>3</sup> and  $\mu = 1.7894 \times 10^{-5}$  Pa s.

For the compressible case the expansibility factor,  $\epsilon$ , was calculated using the equation given in BS EN ISO 5167-1 for Venturi tubes:

$$\epsilon = \left[ \left( \frac{\kappa \tau^{2/\kappa}}{\kappa - 1} \right) \left( \frac{1 - \beta^4}{1 - \beta^4 \tau^{2/\kappa}} \right) \left( \frac{1 - \tau^{(\frac{\kappa-1}{\kappa})}}{1 - \tau} \right) \right]^{1/2}$$

where  $\tau$  is the ratio of the throat and upstream wall pressures at the points specified in the Standard,  $p_t / p_u$ , and  $\kappa$  is the isentropic exponent which for the ideal gas was computed as equal to the ratio of specific heat capacities,  $\gamma = 1.4$ . The numerical results are given in Table 2.

TABLE 2  
COMPARISON OF COMPUTATIONS BETWEEN  
INCOMPRESSIBLE AND COMPRESSIBLE FLOW

	Incompressible	Compressible
C	0.98584	0.98699
$\epsilon$	1.0	0.97783
$p_u$	2018222.35	2018815.58
$p_t$	1941433.40	1938852.10
$\Delta p$	76788.95	79963.48

The discharge coefficient in compressible flow only differs by 0.12 per cent from that computed for incompressible flow. It was therefore concluded that for the same  $Re_D$  the discharge coefficient would be almost the same for compressible or incompressible flow provided the maximum Mach number was always much less than 0.3.

To verify the unstructured mesh technique a comparison was made between the structured and unstructured mesh techniques for incompressible flow. There was a difference in discharge coefficient of only 0.05 per cent between the unstructured mesh at  $Re_D = 2.66 \times 10^6$  and the structured mesh at the same  $Re_D$  obtained by interpolating between the values for  $Re_D = 10^6$  and  $4 \times 10^6$  (assuming a linear dependence on  $\log Re_D$ ).

## 5 EFFECT OF CHANGES IN GEOMETRY

### 5.1 Effect Of Increasing The Angle Of The Divergent Section

A study of the effect on the discharge coefficient of the angle of the divergent section was made by computing the discharge coefficient with included angles for the divergent section of  $11^\circ$  and  $15^\circ$  for  $\beta = 0.4$  and  $0.75$ . These were compared with those obtained for the baseline case (Table 1) which has an included angle of  $7\frac{1}{2}^\circ$ . For confirmation of the pattern the discharge coefficient for a divergent section of included angle  $15^\circ$  was obtained for  $\beta = 0.6$ . Table 3 gives the percentage change in discharge coefficient from the baseline for all the above computations. All the shifts were positive and less than 0.05 per cent.

**TABLE 3**  
**PERCENTAGE SHIFT IN DISCHARGE COEFFICIENT**

$\beta$	$\alpha = 11^\circ$	$\alpha = 15^\circ$
0.4	0.05	0.05
0.6	-	0.02
0.75	0.04	0.02

The results show that an increase in the included angle from  $7\frac{1}{2}^\circ$  to  $15^\circ$  has an insignificant effect on the discharge coefficient.

### 5.2 Effect Of Increasing the Radii Of Curvature

A study of the effect on the discharge coefficient of increasing the radii of curvature at the intersections of the upstream pipe and the convergent,  $R_1$ , of the convergent section and the throat,  $R_2$ , and of the throat and the divergent section,  $R_3$ , was performed.

The baseline computations were performed with  $R_1$ ,  $R_2$ , and  $R_3 = 5$  mm; this was the minimum practicable radius of curvature possible at the time. The Venturi calibrations in water were performed on Venturis manufactured with a specified maximum radius of curvature tolerance of 1mm on all corners.

Computations were performed for Venturi tubes with the maximum radius of curvature permitted by BS EN ISO 5167-1 at a given intersection. For a classical Venturi tube with a machined convergent section the standard gives the following specification:  $R_1 < 0.25D$  and  $R_2$  and  $R_3 < 0.25d$ . Therefore, computations were performed for  $D = 154.04$  mm,  $R_1 = 38.5$  mm for all diameter ratios and  $R_2$  and  $R_3 = 15.4$  mm, 23.1 mm and 28.9 mm for  $\beta = 0.4$ , 0.6 and 0.75 respectively.

The result of these computations gave shifts in the discharge coefficient from the **baseline case** (Table 1) of less than  $\pm 0.025$  per cent. However, where the maximum permissible radii of curvature were used the magnitude of the spikes at the intersections was reduced; for  $\beta = 0.4$  the difference between the static pressure at the wall at intersection  $R_2$  and that at the throat was 29 per cent, a reduction of 12 per cent from the geometry where the radii of curvature were all 5 mm.

## 6 EFFECT OF REYNOLDS NUMBER

Further computations were carried out for  $Re_D = 2 \times 10^5$ ,  $4 \times 10^6$  and  $2 \times 10^7$  and  $\beta = 0.4$ , 0.6 and 0.75 to determine the effect of Reynolds number on discharge coefficient; the results are shown in Table 4, where  $\Delta C_{P,b}$  is the percentage difference between  $C_{CFD}$  (given in Table 4 for each  $Re_D$ ) and the baseline  $C_{CFD}$  (given in Table 1 for  $Re_D = 10^6$ ).

T A B L E 4

EFFECT OF REYNOLDS NUMBER ON DISCHARGE COEFFICIENT

$Re_D$	$2 \times 10^5$		$4 \times 10^6$		$2 \times 10^7$	
$\beta$	$C_{CFD}$	$\Delta C_{P,b}$	$C_{CFD}$	$\Delta C_{P,b}$	$C_{CFD}$	$\Delta C_{P,b}$
0.4	0.98187	<b>-0.28</b>	0.98700	<b>0.24</b>	0.98864	<b>0.41</b>
0.6	0.98290	<b>-0.33</b>	0.98864	<b>0.25</b>	0.99061	<b>0.45</b>
0.75	0.98261	<b>-0.38</b>	0.98879	<b>0.25</b>	0.99078	<b>0.45</b>

On the basis of these computations it is clear that the discharge coefficient is a function of Reynolds number but that the term which describes the dependence on Reynolds number can be assumed not to be a function of  $\beta$ . More work is required to determine the exact functional relationship.

## 7 EFFECT OF ROUGHNESS

BS EN ISO 5167-1<sup>(3)</sup> specifies a maximum limit of upstream pipe roughness of  $k_s/D \leq 10^{-3}$  (where  $k_s$  is the roughness height) on a length at least equal to  $2D$  measured upstream from the classical Venturi tube. It also specifies that the roughness criterion  $R_a$  of the throat and that of the adjacent curvature shall be less than  $10^{-5} d$  and that the divergent section is roughcast. For Venturi tubes with a machined convergent section it specifies that the entrance cylinder and the convergent section shall have a surface finish equal to that of the throat.

For the NEL calibrations the Venturi entrance cylinder, convergent section and throat had a specified maximum value for  $R_a$  of  $0.4 \mu m$  for  $\beta = 0.4$  and  $0.8 \mu m$  for  $\beta = 0.6$  and  $0.75$ . On all other machined surfaces the value of  $R_a$  was  $3.2 \mu m$  for all diameter ratios.

It was expected that the maximum shift in discharge coefficient would occur at the highest Reynolds number. Therefore, at  $Re_D = 2 \times 10^7$ , in addition to the computations with smooth walls, computations were performed for Venturi tubes of different roughnesses for  $\beta = 0.75$  and  $\beta = 0.4$ . To verify this assumption one computation was performed for  $Re_D = 1 \times 10^6$ ,  $\beta = 0.75$ , a smooth inlet, pipe roughness  $R_a = 0.8 \mu m$  for the  $2D$  upstream of the convergent section, the convergent and the throat sections and  $R_a = 3.2 \mu m$  elsewhere; the shift in  $C$  was negligible.

### 7.1 Effect of Roughness for $\beta = 0.75$

For  $\beta = 0.75$  and  $Re_D = 2 \times 10^7$  seven roughness cases were computed.

The first case was computed with a smooth inlet and smooth Venturi tube and given in Table 4.

For the second case a rough upstream pipe was specified ( $k_s/D = 5 \times 10^{-4}$ ). Over the 2D upstream of the entrance cylinder and throughout the Venturi tube smooth walls were specified. This gave a positive shift in discharge coefficient of 0.17 per cent.

The third case was an extreme case where the upstream pipework and the Venturi tube were rough ( $k_s/D = 5 \times 10^{-4}$ ). This gave a shift in discharge coefficient of -1.17 per cent.

Cases 4 to 7 are shown in Fig. 7. The fourth case was a simulation of a typical Venturi tube (same roughness as in experimental tests) with a rough inlet (same as case 2) and gave no shift ( $\Delta C = 0.01$  per cent) in discharge coefficient. The fifth case examined the effect of roughening the entrance section and the convergent section and for a rough inlet gave a shift in discharge coefficient of -0.35 per cent.

Since the effect of a rough inlet was to give a positive shift and the effect of a rough Venturi tube was to give a negative shift in discharge coefficient, the two effects can cancel each other out to some extent. Therefore, in order to determine a reasonable limit for roughness of the Venturi tube the worst case inlet profile is a smooth pipe. The last two cases were computed with a smooth inlet profile. The case where the Venturi tube had the same roughness as that of one of the Venturi tubes in the experiments ( $0.8 \mu\text{m}$  entrance, convergent and throat sections and  $3.2 \mu\text{m}$  elsewhere) gave a shift in discharge coefficient of -0.21 per cent. This roughness of the Venturi tube is acceptable since with the smooth upstream pipe it is being used with the worst case inlet profile; the profile from a rougher pipe would have the effect of decreasing the magnitude of the shift and, as in case 4, an inlet pipe roughness of  $k_s/D = 5 \times 10^{-4}$  gives no shift; this is the zero crossover point and an inlet pipe with a roughness greater than  $k_s/D = 5 \times 10^{-4}$  would give a positive shift.

## 7.2 Effect of Roughness for $\beta = 0.4$

Three roughness cases were computed for  $\beta = 0.4$  and  $Re_D = 2 \times 10^7$ ; these are shown in Fig. 8 as cases 8, 9 and 10. The objective of computing these cases was to determine whether the maximum roughness limits in BS EN ISO 5167-1 for the critical sections of the Venturi tube are adequate. For  $\beta = 0.4$  the maximum permissible roughness is  $R_a = 0.6 \mu\text{m}$  for the convergent and the throat sections. Case 8 with a rough inlet ( $k_s/D = 5 \times 10^{-4}$ ) and smooth Venturi tube proved that the pipe roughness over the 2D upstream of the entrance cylinder has no effect on the discharge coefficient. Case 9 is the maximum permissible roughness for the convergent and the throat sections (i.e.  $R_a = 0.6 \mu\text{m}$ ) and smooth elsewhere. This gave a shift in discharge coefficient of -0.30 per cent. Case 10 specified a rough convergent section and entrance cylinder only and smooth elsewhere; there was no change in discharge coefficient. These results show that the roughness limit for the convergent and for the upstream pipework is too small and for the throat it is too large.

### 7.3 Validation of Roughness Computations

Operational experience has shown that increasing Venturi flowmeter roughness decreases  $C$ . As Venturi roughness increases, the frictional losses and the measured pressure drop for the Venturi increase for a given flowrate and hence  $C$  is reduced. Theoretical analyses lead to the same conclusions. Increasing roughness causes the velocity gradient from the wall to reduce and hence the displacement thickness of the boundary layer to increase. Examination of Hall's equation<sup>(6)</sup>, demonstrates that  $C$  will then be reduced.

These qualitative observations have been validated experimentally by several workers. Schlag<sup>(7)</sup> demonstrated this by artificially roughening the convergent cone of the Venturi and compared the calibration results before and after to discover that  $C$  had decreased. As part of the same programme, he investigated the effect of roughening the upstream pipe. The result was that increasing upstream roughness increased  $C$ . These results are shown in Fig. 9; the black dots correspond to a rough Venturi and the clear dots correspond to a smooth Venturi.

Hutton<sup>(8)</sup> conducted a series of experiments to investigate the effect of roughness on  $C$ : his results can be seen in Fig. 10. It can be seen that increasing Venturi roughness causes  $C$  to fall whereas increasing pipe roughness causes  $C$  to increase. Hutton concludes that if Venturi and upstream pipe are made of the same material, the Venturi roughness dominates and consequently  $C$  will fall with time as the system progressively rusts.

## 8 CONCLUSIONS - SPECIFIC

Baseline discharge coefficients have been computed for  $\beta = 0.4, 0.6$  and  $0.75$  and  $D = 154.04$  mm at a Reynolds number of  $10^6$ . All computations showed unexpected spikes in all the profiles close to the pipe wall along the length of the Venturi tube. These spikes occurred at the intersections of the Venturi sections, in particular at the intersection of the conical convergent and the throat and at the intersection of the throat and the conical divergent sections. These spiky profiles do not just occur along the pipe wall but persist into the flow and decay with distance from the pipe wall; at the centreline all profiles are smooth and there are no spikes.

A comparison with a computation in compressible flow using an unstructured grid showed that there was no compressibility or mesh effect; the shift in discharge coefficient was insignificant and the same spiky profiles were present.

A change in the angle of the divergent section from an included angle of  $7\frac{1}{2}^\circ$  to  $15^\circ$  had no significant effect on the discharge coefficient.

A change in the radii of curvature at the most significant three intersections of the Venturi tube from 5 mm to the maximum permitted in BS EN ISO 5167-1 at a given intersection made no significant difference to the discharge coefficient.

Further Venturi tube discharge coefficients were computed for three values of  $\beta$ , 0.4, 0.6 and 0.75, at Reynolds numbers of  $2 \times 10^5$ ,  $4 \times 10^6$  and  $2 \times 10^7$ . These show that

the discharge coefficient is a function of Reynolds number but the term which describes the dependence can be assumed not to be a function of  $\beta$ .

The study of the effect of pipe roughness shows that discharge coefficients are only affected by pipe roughness at the higher Reynolds numbers. For a Venturi tube with  $\beta = 0.75$  at  $Re_D = 2 \times 10^7$  a rough ( $k_s/D = 5 \times 10^{-4}$ ) inlet pipe has the effect of increasing the discharge coefficient, from the smooth inlet pipe case, by approximately 0.2 per cent. However, a Venturi tube with  $R_a = 0.8 \mu\text{m}$  and a smooth inlet pipe has the effect of decreasing the discharge coefficient, from the smooth Venturi tube case, by 0.2 per cent. For  $\beta = 0.4$  and  $Re_D = 2 \times 10^7$  there is no shift in discharge coefficient for a rough inlet pipe and smooth Venturi tube. The Venturi tube with  $R_a = 0.6 \mu\text{m}$  gives  $\Delta C = -0.3$  per cent; this shift is entirely due to the rough throat.

## 9 CONCLUSIONS - GENERAL

This paper has shown that accurate simulations of flow through flowmeters are possible using CFD. The CFD results of flows through Venturi meters presented in this paper have been extensively verified using recent Venturi calibration data, detailed pressure profile data from the 1960's and surface roughness experiments from the 1950's.

The results showed that at high Reynolds numbers there was a small positive shift in discharge coefficient but nothing like the large shifts obtained when the Shell Venturi meters were calibrated at NEL in high pressure gas. However, the CFD acted as a useful tool in quickly eliminating suspected causes of the phenomenon: it showed that changes in geometry were probably not the cause. It also indicated that separation was probably not the mechanism by which the large shifts occurred. The only part of the Venturi that was not modelled were the pressure tappings, they appear to be the only possible geometrical cause of the problem. Also in the computations an ideal gas model was used and assumptions were made about expansibility. If the cause of the problem was flow related (as opposed to acoustic related) then these were the most likely causes.

The maximum roughness used for the CFD computations are the maximum limits specified in the Standard but further work needs to be done to determine if these are realistic for Venturis in service. The shifts reported in the literature are much larger than those found in the CFD work but the discharge coefficients were obtained from much rougher Venturis. Although roughness effects are understood qualitatively, to date nothing has been found in the literature that presents a general model quantifying the effect of age and roughness on discharge coefficients. This is not surprising as the issue is highly complex because of the vast array of roughening mechanisms and their possible effects on flow through the Venturi.

This work forms the basis of further possible research using CFD on the effect of upstream and Venturi surface roughness on the performance of these meters. The knowledge gained on the effect of surface roughness may also be applicable to ultrasonic flowmeters. The results of this work can also be used to improve the Standard for Venturi meters.

## ACKNOWLEDGEMENT

The authors wish to thank Shell Exploration and Production for their kind permission to publish this paper. In particular they would like to thank Andy Jamieson for his continued support.

## REFERENCES

- 1 DICKINSON and JAMIESON. High accuracy wet gas metering. North Sea Flow Metering Workshop, Bergen, Norway, Oct. 1993.
- 2 MURDOCK, J. W. Two phase flow measurement with orifices. *Journal of Basic Engineering*, Dec. 1962.
- 3 INTERNATIONAL ORGANIZATION FOR STANDARDIZATION. Measurement of fluid flow by means of orifice plates, nozzles and Venturi tubes inserted in circular cross-section conduits running full. BS EN ISO 5167-1, Geneva: International Organization for Standardization, 1991.
- 4 LINDLEY, D. Venturi meters and boundary layer effects. Ph.D. Thesis, University College of South Wales and Monmouthshire, Sept. 1966.
- 5 JAMIESON, A. W., JOHNSON, P. A., SPEARMAN, E. P., and SATTARY, J. A. Unpredicted behaviour of Venturi flowmeter in gas at high Reynolds numbers. North Sea Flow Measurement Workshop, Peebles 1996.
- 6 HALL, G. W. Application of boundary layer theory to explain some nozzle and Venturi flow peculiarities. *Proc. Institute of Mechanical Engineers*. London, Vol 173, No 36, pp 837, 1959.
- 7 SCHLAG, R. Survey of studies of classical Venturi meters at the University of Leige. Flow measurement in closed conduits. *Proc. of a symposium held at the National Engineering Laboratory*. Vol 1, Paper C2, Page 269, Sept. 1960.
- 8 HUTTON, S. P. The prediction of Venturi flowmeter coefficients and their variation with roughness and age. *Proc. Instn. Civ. Engrs.*, Vol 3, Part 3, pp 216, 1954.

## LIST OF FIGURES

- 1 Computed Velocity Profiles Along the Venturi
- 2 Computed Pressure Profiles Along the Venturi

- 3 Computed Pressure Profiles Along the Venturi in the Throat Region
- 4 Lindley (1966). Measured Pressure Profiles Along the Venturi Wall
- 5 Lindley (1966). Measured Pressure Profiles in the Region of the Intersection of the Convergent and Throat Sections for  $Re_d < 300\,000$ .
- 6 Lindley (1966). Measured Pressure Profiles in the Region of the Intersection of the Convergent and Throat Sections for  $Re_d > 300\,000$ .
- 7 Computed Effect of Roughness - Summary of Cases 4 to 7.
- 8 Computed Effect of Roughness - Summary of Cases 8 to 10.

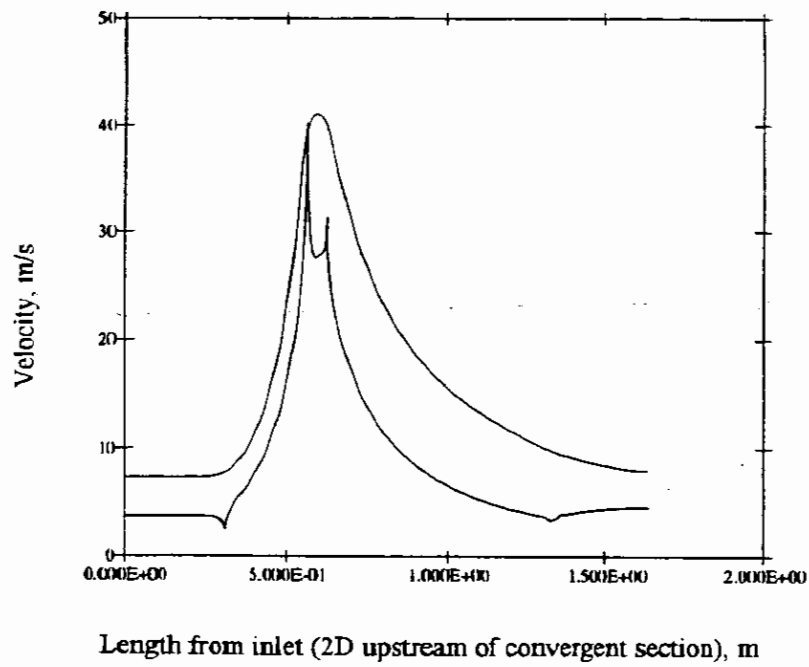


Fig. 1 Computed Velocity Profile Along with Venturi

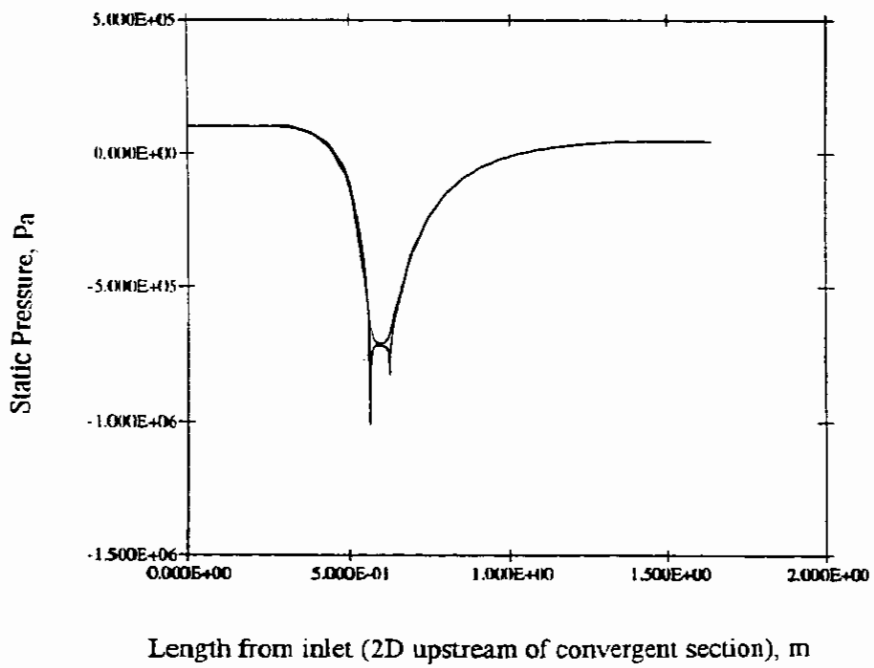


Fig. 2 Computed Pressure Profiles Along with Venturi

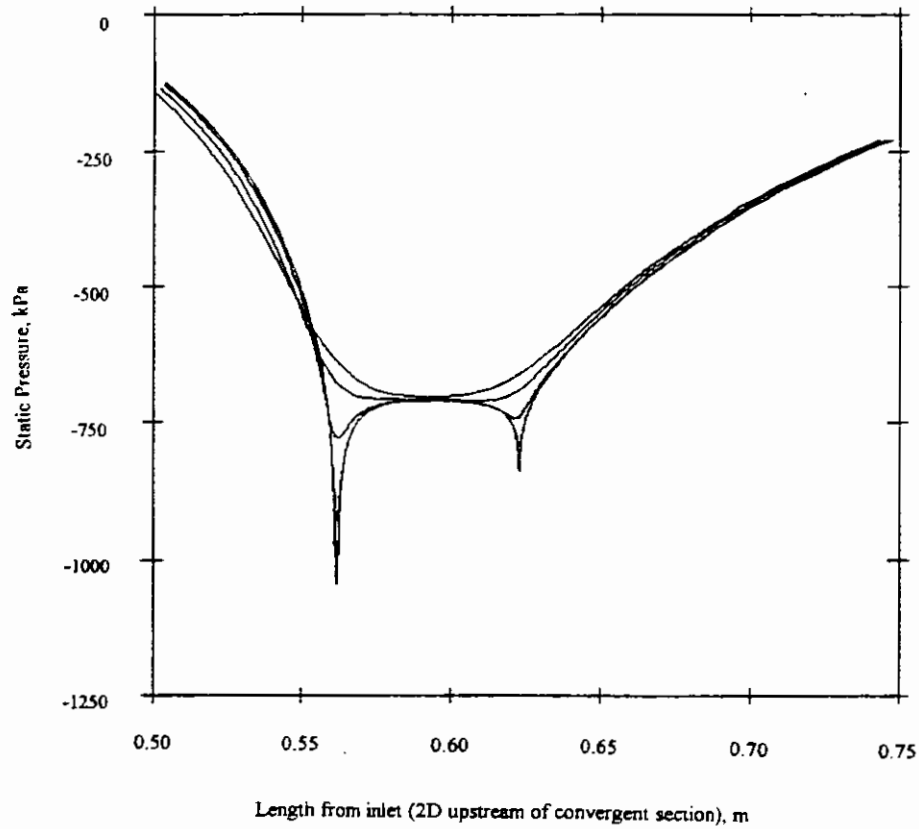


Fig. 3 Computed Pressure Profiles Along the Venturi in the Throat Region

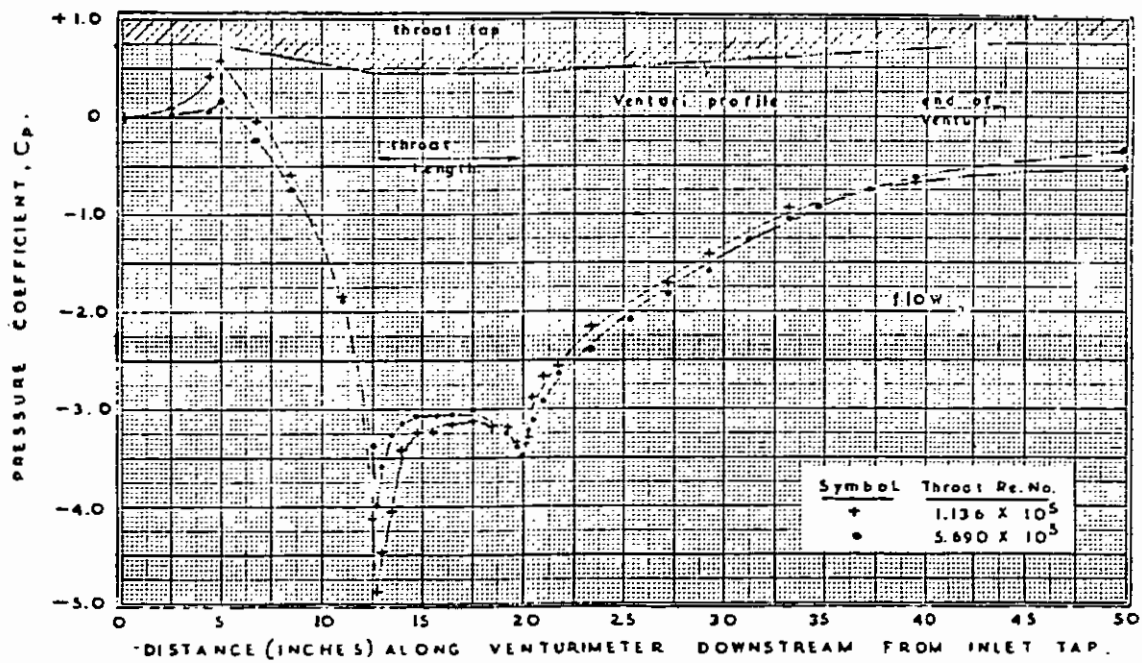


Fig. 4 Lindley (1966). Measured Pressure Profiles Along with Venturi Wall

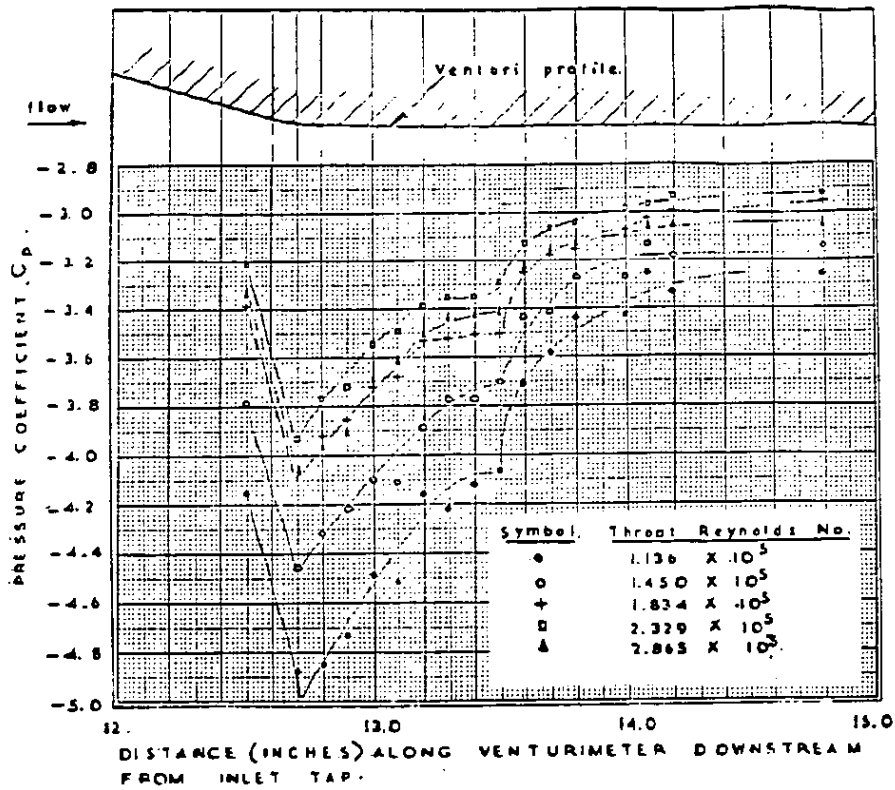


Fig. 5 Lindley (1966). Measured Pressure Profiles in the Region of the Intersection of the Convergent and Throat Sections for  $Re_d < 300\,000$

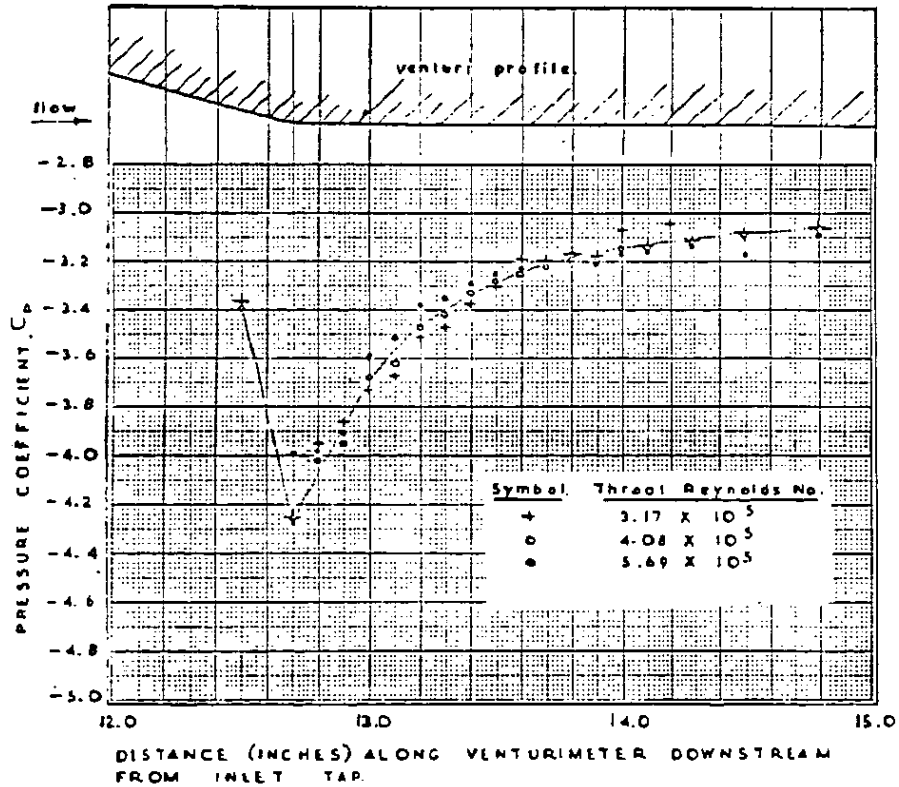
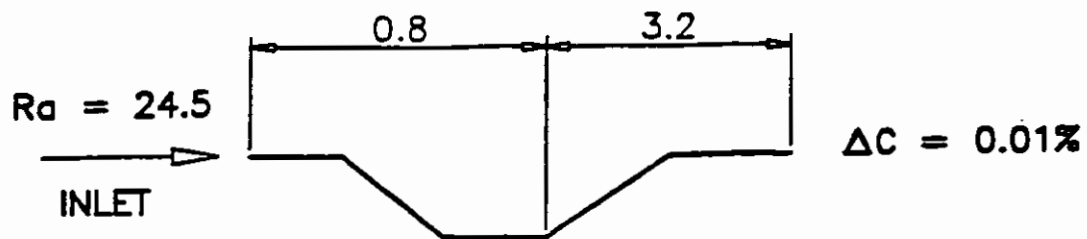
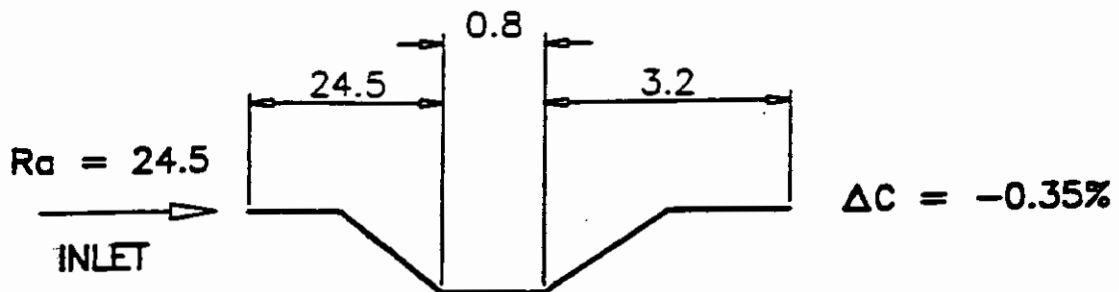


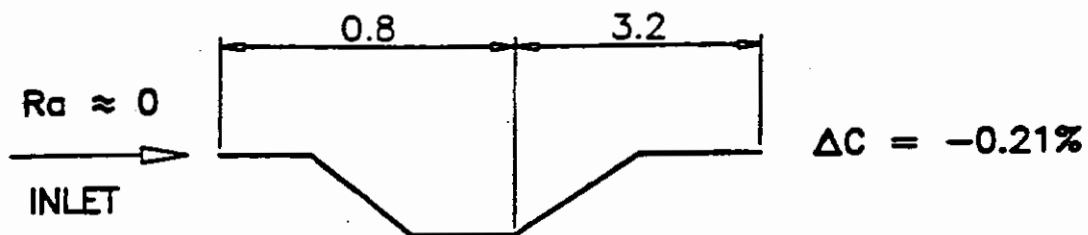
Fig. 6 Lindley (1966). Measured Pressure Profiles in the Region of the Intersection of the Convergent and Throat Sections for  $Re_d > 300\,000$



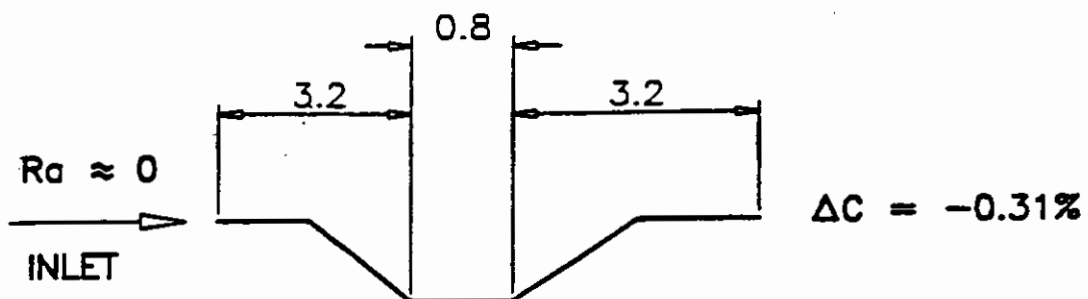
CASE 4: ROUGH INLET, VENTURI AS MANUFACTURED FOR EXPERIMENTS



CASE 5: ROUGH INLET, ROUGH CONVERGENT SECTION



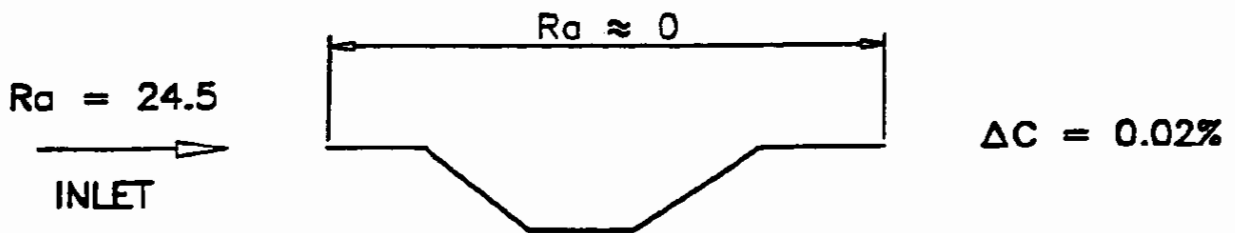
CASE 6: SMOOTH INLET, VENTURI AS MANUFACTURED FOR EXPERIMENTS



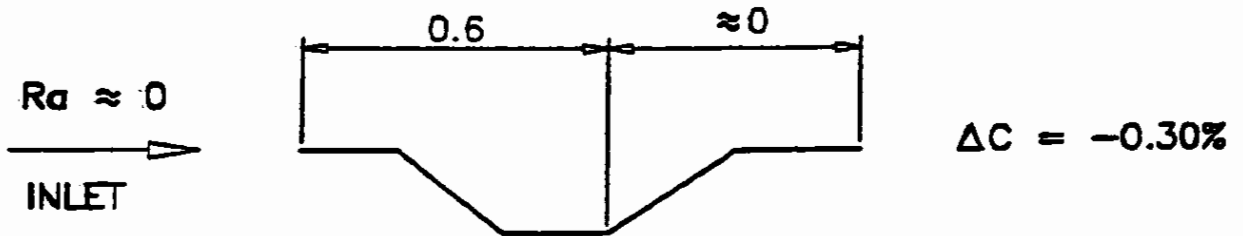
CASE 7: SMOOTH INLET, SLIGHTLY ROUGH CONVERGENT SECTION

Note: All values of  $R_a$  are in  $\mu\text{m}$

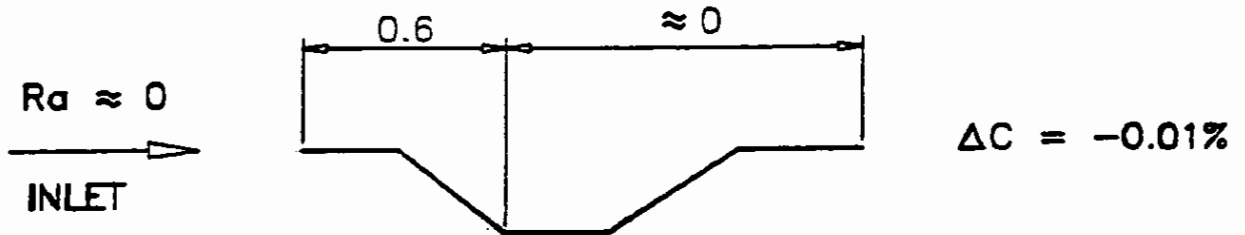
Fig. 7 Computed Effect of Roughness - Summary of Cases 4 to 7



CASE 8: ROUGH INLET, SMOOTH VENTURI



CASE 9: SMOOTH INLET, CONVERGENT & THROAT MAX IN ISO 5167



CASE 10: SMOOTH INLET, CONVERGENT ROUGH VENTURI SMOOTH

Note: All values of Ra are in  $\mu\text{m}$

Fig. 8 Computed Effect of Roughness - Summary of Cases 8 to 10

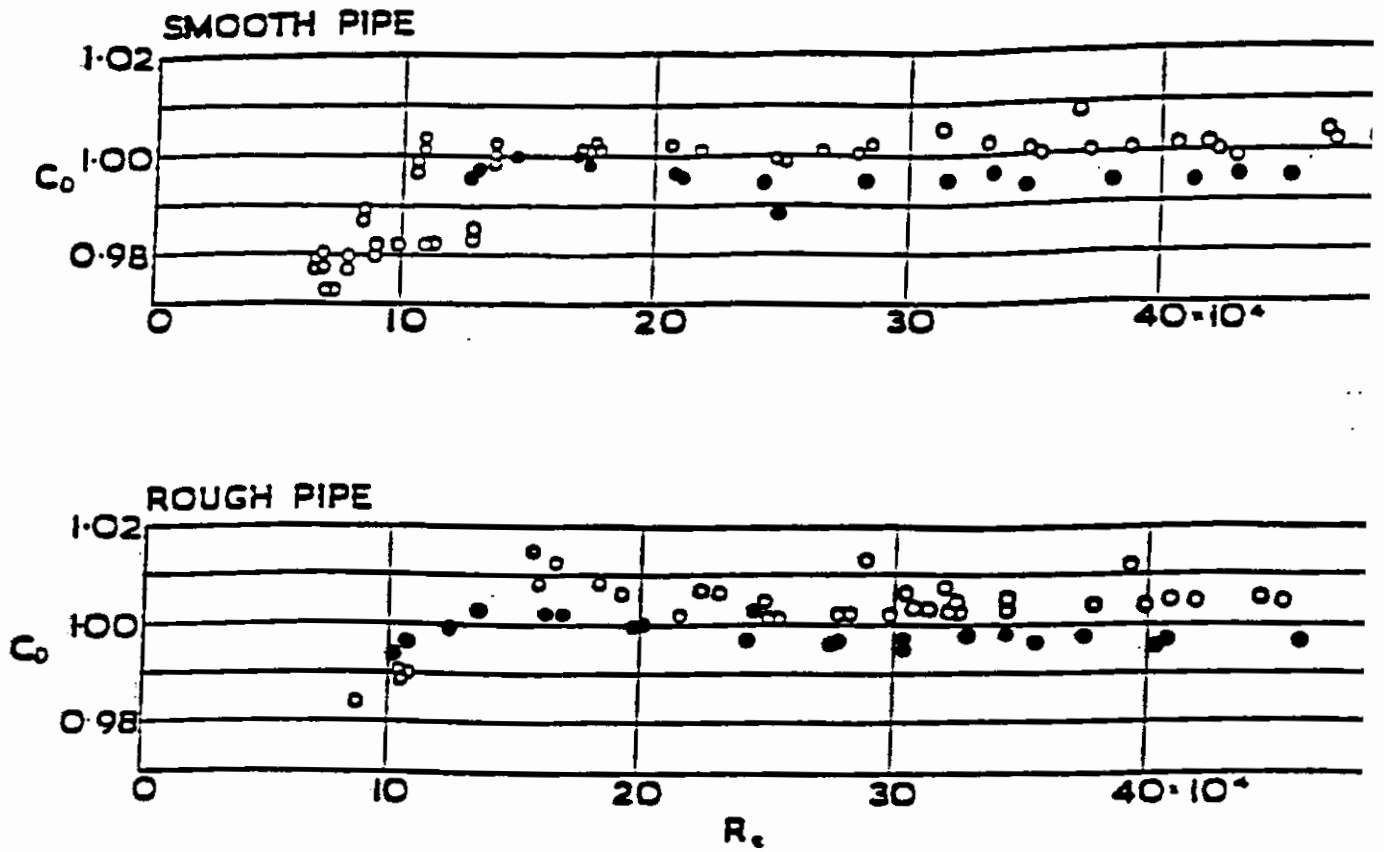


Fig. 9 Schlag (1960). Effect of roughness of convergent cone and upstream pipe

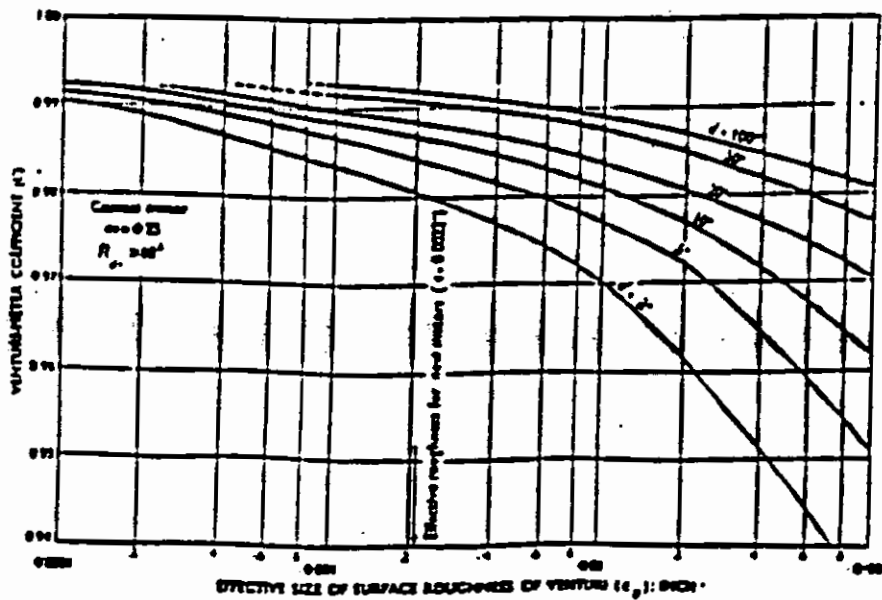


Fig. 10 Hutton (1954). Variation of  $C_d$  with surface roughness